American Research Journal of
Chemical Engineering

ARJ PUBLISHING
Inspiring Research. Shaping Futures

Research Article

Development and Performance Assessment of Emerging Catalytic Materials for Liquid-Phase Refining of Petroleum-Derived Oils

Chunyan Wang[1*], Pengchong Li[2], Yongqin Zhou[3]

[1]Department of Chemistry, Tsinghua University, Beijing 100084, China.
[2]School of Chemistry and Chemical Engineering, Chemistry and Biomedicine Innovation Center, Nanjing University, Nanjing 210023, China.

Correspondence to: Chunyan Wang, Department of Chemistry, Tsinghua University, Beijing 100084, China.

Publication Information: Accepted: May 15, 2026**, Published:** May 22, 2026

Citation: Wang C, et al. Development and Performance Assessment of Emerging Catalytic Materials for Liquid-Phase Refining of Petroleum-Derived Oils. American Research Journal of Chemical Engineering, Vol 1, no. 1, 2026: 1-8.

Copyright © 2026 Wang C, et al. This is an open access article distributed under the Creative Commons Attribution License, which permits unrestricted use, distribution, and reproduction in any medium, provided the original work is properly cited.

Abstract

The upgrading of direct coal liquefaction (DCL) oil requires effective removal of sulfur- and nitrogen-containing compounds, together with the reduction of polycyclic aromatic hydrocarbons. Conventional supported hydrotreating catalysts may experience limitations arising from pore obstruction, active-phase aggregation, and restricted access to catalytic sites. This study compares an unsupported catalyst prepared through a forming route with a supported catalyst produced by conventional impregnation. The investigation examines whether the unsupported active phase retains its chemical identity and dispersion characteristics during catalyst shaping, a feature described here as modularized property. Structural and textural characteristics were examined using X-ray diffraction, nitrogen adsorption, scanning electron microscopy, high-angle annular dark-field scanning transmission electron microscopy, and carbon monoxide chemisorption. Catalytic performance was evaluated through hydrodesulfurization, hydrodenitrogenation, and hydrodearomatization measurements. The forming-based catalyst exhibited improved retention of its initial morphology and a more favourable pore structure before presulfidation. After sulfide formation, the proportion of slabs containing more than two stacked layers was approximately 1.5 times that observed for the impregnation-derived catalyst. The unsupported catalyst also showed higher hydrotreating activity and maintained stable performance during a 120-hour test.

Keywords: Unsupported Catalysts; Modularized Active Phase; Coal-Derived Liquids; Hydrotreating; Active-Site Dispersion; Hydrodesulfurization; Hydrodenitrogenation; Hydrodearomatization; Catalyst Forming.

INTRODUCTION

Increasingly demanding fuel-quality requirements have encouraged the development of catalytic technologies capable of reducing harmful compounds in petroleum-derived and alternative liquid fuels. Catalytic treatment plays an important role in controlling emissions associated with transportation fuels and improving the quality of refinery products [1]. Secondary-processing streams frequently contain complex mixtures of sulfur compounds, nitrogen-containing molecules, and aromatic constituents, making their conversion into cleaner fuel products a demanding industrial task [2]. Hydrotreating is widely used to improve the quality of liquid hydrocarbon feedstocks. Its effectiveness depends on catalyst composition, pore architecture, active-phase accessibility, hydrogen availability, and operating conditions. The performance of nickel–molybdenum-based catalysts can also vary with the nature of the support and the chemical characteristics of the feedstock [3].

Unsupported catalysts have been developed to increase the proportion of catalytically active material and reduce dependence on conventional porous supports. Bulk metal-containing formulations can provide a high concentration of active components, making them attractive candidates for hydroprocessing applications [4]. Research into unsupported nickel-containing molybdenum catalysts has demonstrated that their composition and preparation conditions influence hydrodesulfurization performance.

The catalytic behaviour of unsupported materials is strongly affected by the morphology of the sulfide phase. Changes in molybdenum disulfide slab dimensions, stacking, and dispersion can alter the number and accessibility of active sites. The morphology of unsupported cobalt–molybdenum sulfides has therefore been investigated in relation to selective sulfur removal from gasoline-range feedstocks [5].

High-surface-area bulk nickel–molybdenum–tungsten formulations have also been examined as alternatives to conventional supported catalysts. Their preparation and structural properties demonstrate the importance of controlling particle growth and maintaining accessible surface regions [6]. In addition, alternative precursor routes have been investigated to improve the formation of catalytically active nickel–molybdenum phases. Multimetallic bulk catalysts prepared using structural templates have shown that precursor architecture can influence the final catalytic properties. The selection of metal composition and synthesis conditions consequently remains important when designing catalysts for the removal of refractory sulfur-containing molecules [7]. Further studies of zinc-containing multimetallic formulations have demonstrated that changes in composition can modify the hydrodesulfurization behaviour of bulk catalyst systems.

Despite these developments, the preparation of an unsupported catalyst in powder form does not automatically guarantee that its structure will remain unchanged during subsequent shaping. A suitable forming procedure must preserve the distribution and chemical characteristics of the active phase while producing a mechanically and texturally appropriate catalyst body. Shaped bulk-catalyst preparation has therefore become an important consideration in the development of industrially relevant unsupported formulations [8]. Organic additives have been used to regulate particle growth and reduce aggregation during catalyst synthesis. Polyvinylpyrrolidone-assisted preparation, for example, has been investigated as a route for controlling the dispersion of unsupported nickel–molybdenum components. Sol–gel synthesis has also been explored as a means of constructing bulk catalyst structures with improved hydrosulfurization characteristics [9].

The sulfiding stage is another important factor governing the final catalyst architecture. Changes in sulfiding conditions can affect sulfide morphology and the resulting hydrotreating performance. Thermal treatment before sulfiding may also influence the structure and activity of unsupported nickel–molybdenum formulations. Adjusting the chemical composition of the active phase provides an additional route for modifying hydrogenation behaviour [10]. The present study examines the structural and catalytic differences between an unsupported catalyst prepared through a forming process and a supported catalyst produced through conventional impregnation. The central concept is the retention of active-phase characteristics during shaping, referred to as the modularized property. This concept encompasses the ability of the active phase to maintain its chemical identity and dispersibility under forming conditions.

The comparison focuses on crystal structure, particle morphology, pore-size distribution, sulfide-layer characteristics, and hydrotreating performance. The results are used to examine how preparation methodology influences active-phase accessibility and the removal of sulfur, nitrogen, and polycyclic aromatic compounds from the investigated liquid feedstock.

MATERIALS AND METHODS

Catalyst Preparation and Comparative Design

Two catalyst preparation routes were compared. The unsupported catalyst was produced through a forming process, whereas the supported catalyst was prepared by conventional impregnation. The samples were examined before and after the relevant preparation and presulfidation stages [11]. The sample designations used in the original investigation were retained to preserve consistency between the characterization results and the reported figures:

- **UAP:** Unsupported active-phase precursor.
- **UC:** Unsupported catalyst after forming.
- **UC-S**: Unsupported catalyst after sulfiding.
- **CS:** Catalyst support before impregnation.
- **SC:** Supported catalyst after impregnation.
- **SC-S:** Supported catalyst after sulfiding.

The comparison was designed to determine whether the unsupported active phase retained its structural and morphological characteristics during catalyst forming and whether these characteristics influenced the final sulfide architecture.

X-Ray Diffraction Analysis

Powder X-ray diffraction measurements were performed using a Rigaku SmartLab 3KW diffractometer equipped with Cu Kα radiation. The instrument operated at 40 kV

 © 2026 Wang C

and 30 mA. Diffraction patterns were collected for UAP, UC, CS, SC, UC-S, and SC-S. The measurements were used to examine differences in crystalline structure associated with catalyst preparation and presulfidation [12].

Surface Area and Pore-Structure Measurements

Nitrogen adsorption measurements were carried out using a Micromeritics ASAP 2460 surface-area and porosity analyser. Specific surface areas were calculated using the Brunauer–Emmett–Teller method.

The BET calculation was performed over the relative-pressure interval:

$0.05 \leq P/P_0 \leq 0.30$

at 77 K.

Total pore volume was obtained from the single-point adsorption measurement near the maximum relative pressure. Pore-size distributions were evaluated using the Barrett–Joyner–Halenda desorption procedure. The measurements were used to compare changes in pore structure before and after catalyst preparation and presulfidation [13].

Scanning Electron Microscopy

Surface morphology was examined using a JEM7610F scanning electron microscope. Micrographs were obtained for UAP, UC, UC-S, CS, SC, and SC-S. The comparison between UAP and UC was used to assess whether the unsupported active-phase clusters retained their morphology during forming. The supported samples were also examined to identify structural changes associated with impregnation and subsequent sulfiding.

HAADF-STEM and Elemental Mapping

High-angle annular dark-field scanning transmission electron microscopy and elemental mapping were conducted using a JEM-ARM200F NEOARM electron microscope equipped with a probe corrector. Measurements were performed at an accelerating voltage of 200 kV [14]. These analyses were used to investigate active-phase distribution and sulfide-particle characteristics.

Carbon Monoxide Chemisorption

Carbon monoxide chemisorption measurements were performed using a Micromeritics Chemisorb HD88 gas-adsorption system. The catalyst sample was placed in a quartz reactor and pretreated in a 10% H_2/Ar mixture at 450°C for three hours. Following pretreatment, the sample was cooled under helium. Pulses of 10% CO/He were then introduced through a loop tube using helium as the carrier gas at a flow rate of 25 cm^3 (NTP) min^{-1}. Measurements were conducted at 30°C. The chemisorption procedure was used to examine the accessible surface sites of the catalyst materials.

Hydrotreating Performance Evaluation

Catalytic performance was evaluated through three principal reactions:

- Hydrodesulfurization (HDS), assessed through changes in sulfur concentration.
- Hydrodenitrogenation (HDN), assessed through changes in nitrogen concentration.
- Hydrodearomatization (HDAr), assessed through changes in polycyclic aromatic hydrocarbon content.

The supported sulfided catalyst SC-S and unsupported sulfided catalyst UC-S were compared at different reaction temperatures. Feed and product properties were recorded to evaluate the influence of catalyst preparation route on the removal of sulfur, nitrogen, and aromatic compounds.

Long-Term Stability Assessment

A stability experiment was conducted for 120 hours at 320°C under constant weight hourly space velocity. The performance of both catalysts was monitored throughout the test. The recorded product properties included sulfur concentration, nitrogen concentration, and PAH conversion. These measurements were used to examine whether the activity difference between the two preparation routes was maintained during extended operation.

PAH Conversion Calculation

The conversion of polycyclic aromatic hydrocarbons was calculated from the feed and product concentrations using:

$$X_{PAH}=[1-C_{-PAH,produc}t/C_{PAH,feed}]\times 100$$

where $C_{PAH,feed}$ and $C_{PAH,product}$ represent the PAH concentrations in the initial feed and final product, respectively.

RESULTS

Influence of Preparation Route on Crystal Structure

X-ray diffraction patterns were used to examine structural differences between the unsupported and supported catalyst preparation routes. The comparison included UAP, UC, CS, SC, UC-S, and SC-S. The diffraction patterns of UAP and UC displayed similar characteristic features. However,

 © 2026 Wang C

the diffraction intensity of UC was lower than that of UAP. This observation indicates that the forming process influenced the diffraction response without producing a major change in the principal crystalline characteristics of the unsupported active-phase precursor.

The similarity between the two patterns supports the interpretation that the unsupported active phase retained important structural features during shaping. In contrast, the supported samples represented a different preparation pathway in which the active components were introduced into the support through impregnation (Figure 1).

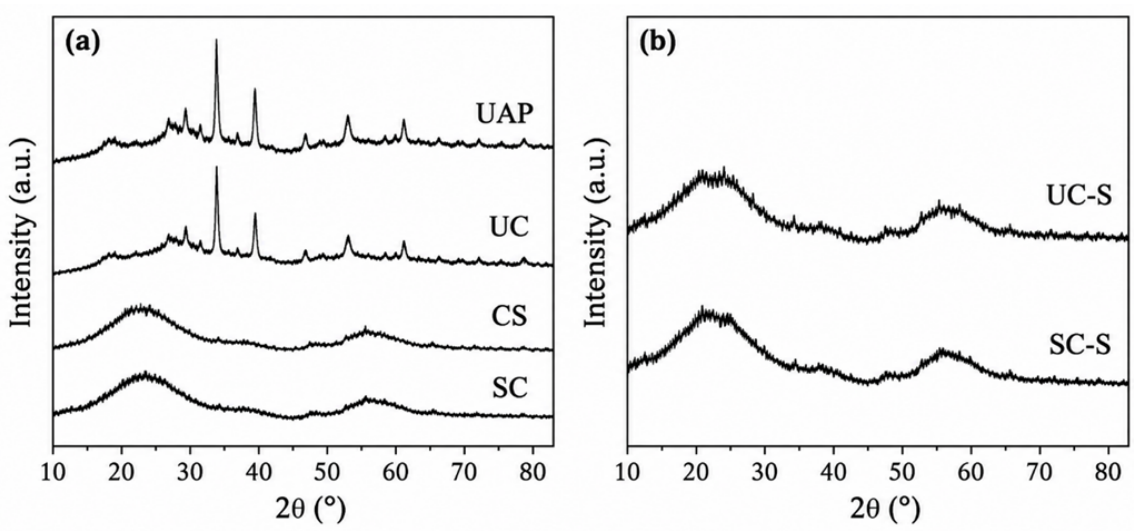


Figure 1: X-ray diffraction profiles of the catalyst precursors and prepared materials: (a) UAP, UC, CS, and SC; (b) UC-S and SC-S.

Recommended presentation: Retain the original diffraction patterns and clearly distinguish each sample using consistent line styles and a readable legend.

Surface Morphology and Active-Phase Retention

Scanning electron microscopy was used to examine the morphological characteristics of the catalyst materials. The UAP sample contained active-phase clusters with reported diameters of approximately 27–29 nm. These clusters consisted of smaller constituent particles and displayed surface irregularities [15]. The comparison between UAP and UC showed that the cluster morphology was substantially retained after the forming process. This observation indicates that the active-phase arrangement was not extensively disrupted during shaping.

The preservation of these clusters provides evidence for the proposed modularized property. In this context, the term describes the retention of the active phase's principal structural and dispersion characteristics during the forming operation. The morphology of the supported samples differed from that of the unsupported materials. These differences were associated with the introduction of the active components into the support and the subsequent treatment stages. Recommended presentation: Arrange the six original micrographs in a clearly labelled panel layout, with identical image scaling wherever possible.

Changes in Pore-Size Distribution

The pore-size distributions of the catalyst materials were examined before and after preparation and presulfidation. The UAP precursor exhibited a relatively broad pore-size distribution, indicating that its initial cluster arrangement did not produce a highly uniform pore structure. Following forming, the UC sample displayed a more concentrated pore-size distribution. This change suggests that the shaping procedure generated a more defined framework within the unsupported catalyst [16]. A different pattern was observed during the impregnation route. Comparison of CS and SC showed a reduction in the contribution of pores larger than 3.8 nm, with a pronounced change around 4.8 nm. The observed decrease is consistent with the presence of impregnation-derived material within the support pores.

Presulfidation also modified the pore structure of both cata-

 © 2026 Wang C

lyst systems. For UC-S, the original framework was affected, particularly in the approximate pore-size interval of 4.3–6.5 nm. In SC-S, enlargement of the active-phase clusters was associated with changes in the 4.3–7.8 nm pore-size region [17]. These observations indicate that the preparation route influences the pore structure before and after sulfide formation. The forming process produced a more concentrated pore distribution in UC, whereas impregnation altered the existing support pore structure through the introduction of the active components (Figure 2).

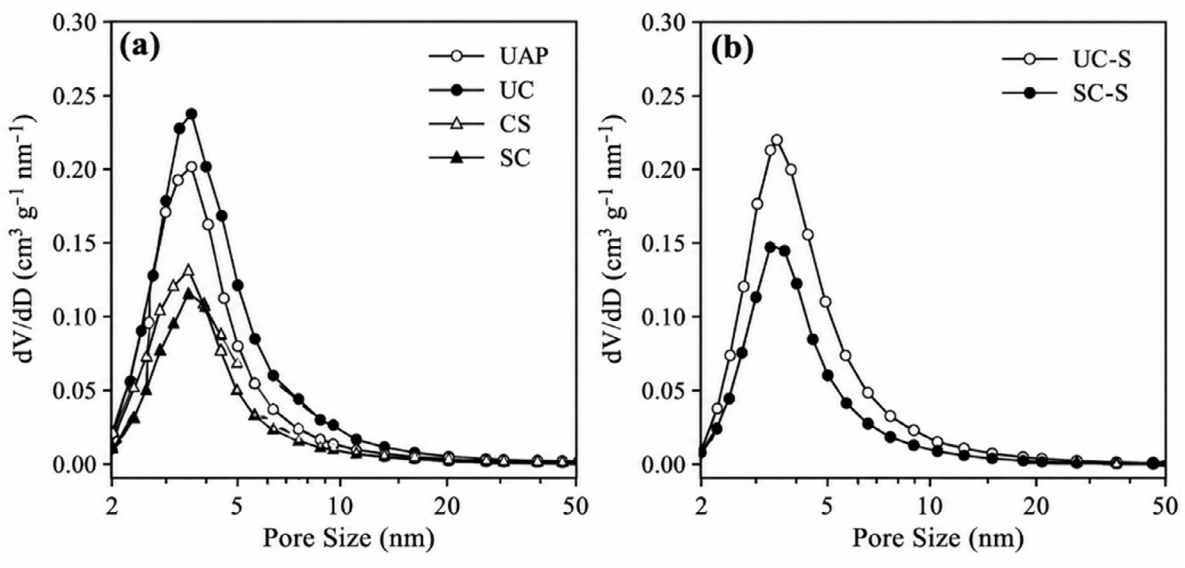


Figure 2: Pore-size distribution profiles of UAP, UC, CS, SC, UC-S, and SC-S before and after presulfidation.

Comparison of Sulfide-Phase Stacking

The sulfide structures were examined to determine how the preparation route influenced active-phase stacking. The forming process increased the distribution ratio of sulfide slabs containing more than two stacked layers. The reported proportion of these multilayer structures in the forming-derived catalyst was approximately 1.5 times that of the catalyst prepared through impregnation. This difference suggests that the preparation route influenced the development of the final sulfide architecture. The stacking characteristics are relevant because the arrangement of sulfide layers affects the structural features of the active phase. The comparison therefore provides an additional basis for examining the relationship between catalyst preparation and catalytic performance.

DISCUSSION

Feedstock and Product Characteristics

The comparison includes sulfur, nitrogen, and PAH concentrations for the supported and unsupported catalyst systems (Table 1) [18].

Table 1: Comparison of feedstock composition and product quality obtained using SC-S and UC-S at 340°C.

Property	Initial Feed	SC-S Product	UC-S Product
Sulfur content (ppm)	1465	24.8	4.4
Nitrogen content (ppm)	810	1.4	1.2
PAH content (wt%)	33.0	12.8	11.9

At 340°C, the UC-S catalyst produced a liquid product with lower sulfur and nitrogen concentrations than the SC-S catalyst. The PAH concentration was also lower for UC-S.

The sulfur concentration decreased from 1465 ppm in the feed to 4.4 ppm with UC-S, compared with 24.8 ppm using SC-S. Nitrogen concentration decreased to 1.2 ppm with UC-S and 1.4 ppm with SC-S. The product obtained with UC-S also contained 11.9 wt% PAHs, compared with 12.8 wt% for SC-S. These measurements demonstrate the higher hydrotreating activity of the unsupported catalyst under the reported comparison conditions.

 © 2026 Wang C

Temperature-Dependent HDS and HDN Performance

The sulfur and nitrogen measurements obtained at different reaction temperatures showed that the unsupported catalyst achieved product-quality levels comparable to those obtained using the supported catalyst at lower operating temperatures. At 300°C, UC-S produced a sulfur concentration of 33.0 ppm and a nitrogen concentration of 5.7 ppm. For SC-S, the corresponding concentrations at 320°C were 33.2 ppm and 4.7 ppm. The sulfur and nitrogen results for UC-S at 320°C were also reported to be close to those obtained with SC-S at 340°C. These comparisons indicate that the unsupported catalyst achieved comparable HDS and HDN performance at a reaction temperature approximately 20°C lower across the reported operating range.

The observed temperature difference is relevant to catalyst evaluation because it demonstrates that the preparation route can influence the operating conditions required to achieve similar product properties.

Hydrodearomatization Performance

The PAH conversion results demonstrated higher hydrodearomatization activity for UC-S than for SC-S at the evaluated temperatures. The difference between the catalysts became more pronounced as the reaction temperature decreased from 340°C to 280°C. At 280°C, the unsupported catalyst showed an approximately 10% higher PAH conversion than the supported catalyst. This result indicates that the forming-derived catalyst maintained an advantage in the conversion of aromatic compounds under the reported lower-temperature conditions.

$X_{PAH}=[1-PAH_{product}/PAH_{feed}]\times100$

Recommended presentation: Use a black-and-white grouped bar chart with reaction temperature on the horizontal axis and PAH conversion (%) on the vertical axis. Use separate bar patterns for SC-S and UC-S.

Relationship Between Pore Architecture and Catalytic Activity

The catalytic performance differences can be considered in relation to the pore structures produced by the two preparation methods. The forming process generated a more concentrated pore-size distribution in UC before presulfidation. Such a framework may provide more accessible transport pathways for relatively large sulfur-containing, nitrogen-containing, and aromatic molecules [19].

In the supported catalyst, the impregnation-derived material occupied part of the original support pore volume. The reduction in pore contribution around 4.8 nm suggests that the introduction of the active components altered the available pore structure. Subsequent presulfidation further changed the textural characteristics of both materials. The observed changes in pore dimensions and active-phase clusters provide a possible explanation for the differences in catalytic performance (Table 2).

Table 2: Comparative Assessment of Emerging Catalytic Materials for Liquid-Phase Refining of Petroleum-Derived Oils.

Catalytic Material	Active Components	Main Catalytic Function	Important Properties to Evaluate	Performance Indicators
Nickel–Molybdenum Catalysts (NiMo)	NiO and MoO_3 precursors	Hydrodesulfurization and hydrodenitrogenation	Active-site dispersion, surface area, acidity	Sulfur removal, nitrogen reduction
Cobalt–Molybdenum Catalysts (Co–Mo)	CoO and MoO_3 precursors	Removal of sulfur-containing compounds	Sulfide formation, pore structure, thermal stability	Desulfurization efficiency, product quality
Nickel–Tungsten Catalysts (Ni–W)	NiO and WO_3 precursors	Hydrocracking and hydrogenation	Metal distribution, pore accessibility, acidity	Conversion efficiency, hydrogen consumption
Zeolite-Based Catalysts	ZSM-5, Y-zeolite, and related materials	Cracking and molecular restructuring	Pore dimensions, acid-site density, structural stability	Product selectivity, liquid yield
Mesoporous Silica Catalysts	Modified silica and supported metals	Adsorption and catalytic conversion	Pore volume, surface area, metal dispersion	Conversion, adsorption capacity

 © 2026 Wang C

Metal Oxide Catalysts	NiO, ZnO, CeO_2, and mixed oxides	Oxidation and removal of selected impurities	Oxygen mobility, surface activity, regeneration ability	Impurity removal, catalyst reusability
Carbon-Supported Catalysts	Activated carbon and supported transition metals	Hydrogenation and impurity conversion	Surface functionality, porosity, metal dispersion	Conversion rate, catalyst lifetime

The combined structural and catalytic observations suggest that the forming route influenced both the arrangement of the active phase and the accessibility of the catalyst structure. These features may contribute to the improved HDS, HDN, and HDAr performance of UC-S.

Long-Term Catalytic Stability

A 120-hour stability test was conducted at 320°C under constant weight hourly space velocity. Both catalysts maintained stable catalytic performance during the reported operating period [20]. The unsupported catalyst retained its activity advantage over the supported catalyst throughout the test. The sulfur concentration in the product obtained using UC-S remained below 5 ppm, while the nitrogen concentration remained below 1.3 ppm. PAH conversion was maintained at approximately 68%.

These results demonstrate that the higher activity of UC-S was not restricted to the initial catalytic evaluation. The sustained performance during the 120-hour experiment supports the potential of the forming-based preparation route for further hydrotreating investigations.

Interpretation of the Modularized Property

The structural comparison indicates that the unsupported active-phase precursor retained its principal cluster morphology during catalyst forming. The preservation of the active-phase arrangement, together with the changes observed in pore distribution and sulfide stacking, provides experimental support for the modularized-property concept. In this study, modularized property refers to the ability of the active phase to retain its chemical and dispersion characteristics during shaping. The concept is relevant because catalyst forming may otherwise cause particle aggregation, structural rearrangement, or changes in active-site accessibility.

The results suggest that maintaining active-phase characteristics during shaping can influence the final catalyst architecture and its hydrotreating performance. However, the contribution of each individual structural feature would require further quantitative investigation to establish the relationship between active-phase retention, pore accessibility, and catalytic activity [21].

The comparison of the two catalyst preparation routes demonstrates that the method used to introduce and shape the active phase can influence the final catalyst structure and performance. The unsupported catalyst retained much of its initial morphology after forming, whereas the supported catalyst experienced changes associated with impregnation and subsequent sulfiding.

The preservation of the unsupported active-phase clusters is consistent with the proposed modularized-property concept. Rather than treating the active phase and the forming operation as independent preparation stages, this concept considers whether the active material can maintain its essential structural characteristics throughout shaping. The pore-size results provide further information about the differences between the preparation routes. The forming process produced a more concentrated pore-size distribution in UC, while impregnation reduced the contribution of selected pores in the support. These differences may affect the movement of larger reactant molecules through the catalyst structure [22].

The catalytic measurements support this interpretation. UC-S achieved lower sulfur, nitrogen, and PAH concentrations than SC-S under the reported comparison conditions. It also maintained higher PAH conversion at lower reaction temperatures. These results are consistent with the established relationship between hydrotreating catalyst structure, active-phase accessibility, and the conversion of complex hydrocarbon feedstocks.

CONCLUSION

This study compared unsupported and supported hydrotreating catalysts prepared through forming and conventional impregnation routes. The results indicate that the unsupported active phase retained much of its initial cluster morphology during shaping, supporting the proposed modularized-property concept. The forming process also produced a more concentrated pore-size distribution before presulfidation, whereas impregnation altered the original support pore structure. Following sulfiding, the unsupported catalyst contained approximately 1.5 times the proportion of slabs with more than two stacked layers compared with the impregnation-

 © 2026 Wang C

derived material. Catalytic testing showed improved sulfur, nitrogen, and PAH removal with UC-S under the reported conditions. Its activity advantage was also maintained during the 120-hour stability experiment at 320°C. These findings indicate that preserving active-phase characteristics during catalyst forming can influence structural development and hydrotreating performance. Further investigations involving different feedstocks, extended operating periods, and quantitative active-site measurements are needed to establish the wider applicability of this preparation strategy.

REFERENCES

1. Dey S, Mehta NS. Automobile pollution control using catalysis. Resources, Environment and Sustainability. 2020;2:100006.
2. Betancourt P, Marrero S, Pinto-Castilla S. V–Ni–Mo sulfide supported on Al_2O_3: Preparation, characterization and LCO hydrotreating. Fuel Processing Technology. 2013;114:21–25.
3. Vozka P, Orazgaliyeva D, Šimáček P, et al. Activity comparison of Ni-Mo/Al_2O_3 and Ni-Mo/TiO_2 catalysts in hydroprocessing of middle petroleum distillates and their blend with rapeseed oil. Fuel Processing Technology. 2017;167:684–694.
4. Soled SMSL, Krikak R, Vroman H, et al. Nickel molybdungstate hydrotreating catalysts. Patent. 2001;US Patent Application 09/518,741.
5. Liu H, Liu CG, Yin CL, et al. Preparation of highly active unsupported nickel-zinc-molybdenum catalysts for the hydrodesulfurization of dibenzothiophene. Applied Catalysis B: Environmental. 2015;174:264–276.
6. Li P, Chen Y, Zhang C, et al. Highly selective hydrodesulfurization of gasoline on unsupported Co-Mo sulfide catalysts: Effect of MoS_2 morphology. Applied Catalysis A: General. 2017;533:99–108.
7. Yu HB, Zhang JC, Nan J, et al. Synthesis and hydrodesulfurization performance of bulk Ni-Mo-W catalyst with high surface area. Advances in Chemical, Material and Metallurgical Engineering. 2013:604–607.
8. Liu H, Yin CL, Zhang HY, Liu CG. Sustainable synthesis of ammonium nickel molybdate for hydrodesulfurization of dibenzothiophene. Chinese Journal of Catalysis. 2016;37:1502–1512.
9. Chen YD, Wang L, Zhang YL, et al. A new multi-metallic bulk catalyst with high hydrodesulfurization activity of 4,6-DMDBT prepared using layered hydroxide salts as structural templates. Applied Catalysis A: General. 2014;474:69–77.
10. Chen YD, Wang L, Liu XY, et al. Hydrodesulfurization of 4,6-DMDBT on multi-metallic bulk catalyst NiAlZnMoW: Effect of Zn. Applied Catalysis A: General. 2015;504:319–327.
11. Eijsbouts S, Leliveld B, Sitters J, et al. Process for the preparation of a shaped bulk catalyst. Patent PCT/EP2006/010293. 2008.
12. Liu H, Liu Q, Zhang J, et al. PVP-assisted synthesis of unsupported NiMo catalysts with enhanced hydrosulfurization activity. Fuel Processing Technology. 2017;160:93–101.
13. Zhang D, Xu Y, Li M, Hou K. Synthesis of Mo-Ni bulk catalyst by sol-gel method and its hydrosulfurization performance. Petroleum Processing and Petrochemicals. 2016;47:67–73.
14. Yin CL, Wang YY, Xue SS, et al. Influence of sulfidation conditions on morphology and hydrotreating performance of unsupported Ni-Mo-W catalysts. Fuel. 2016;175:13–19.
15. Liu H, Yin CL, Liu B, et al. Effect of calcination temperature of unsupported NiMo catalysts on the hydrosulfurization of dibenzothiophene. Energy & Fuels. 2014;28:2429–2436.
16. Li R, Guan Q, Wei R, et al. A potential regularity for enhancing the hydrogenation properties of Ni_2P. The Journal of Physical Chemistry C. 2015;119:2557–2565.
17. Topsøe H, Clausen BS, Massoth FE. Hydrotreating catalysis: Science and technology. Berlin: Springer; 1996.
18. Brunauer S, Emmett PH, Teller E. Adsorption of gases in multimolecular layers. Journal of the American Chemical Society. 1938;60:309–319.
19. Barrett EP, Joyner LG, Halenda PP. The determination of pore volume and area distributions in porous substances. Journal of the American Chemical Society. 1951;73:373–380.
20. Daage M, Chianelli RR. Structure-function relations in molybdenum sulfide catalysts: The “rim-edge” model. Journal of Catalysis. 1994;149:414–427.
21. Speight JG. The chemistry and technology of petroleum. 5th ed. Boca Raton: CRC Press; 2014.
22. Bartholomew CH. Mechanisms of catalyst deactivation. Applied Catalysis A: General. 2001;212:17–60.

 © 2026 Wang C